

Balancing Activity and Stability in Phenol Oxidation via In Situ H₂O₂ Generation Over Fe-Modified AuPd Catalysts

Rong-Jian Li,^[a] Richard J. Lewis,^{*,[a]} David J. Morgan,^[a, b] Ella Kitching,^[c] Thomas Slater,^[c] and Graham J. Hutchings^{*,[a]}

Harnessing the in situ generation of hydrogen peroxide (H₂O₂) and associated reactive oxygen species (ROS) from molecular hydrogen (H₂) and oxygen (O₂) offers a powerful and sustainable alternative to conventional oxidative treatments for water purification. In this contribution, we explore the potential of AuPdFe-based catalysts to achieve the in situ, oxidative degradation of phenol, a widely studied representative organic pollutant. By finely tuning the AuPd/Fe ratio, it is possible to balance H₂O₂ synthesis with Fe-mediated ROS generation, achieving effi-

cient phenol degradation and high selectivity toward deeply oxidized products. The optimized catalyst formulation outperforms its bimetallic counterpart by a factor of 10 in conversion efficiency. However, this enhanced activity comes at a cost, with the formation of strongly oxidized species such as formic, oxalic, and malonic acids resulting in the leaching of the active metal components, highlighting a critical trade-off between catalytic performance and long-term stability, particularly in the presence of highly concentrated chelating agents.

1. Introduction

Persistent organic contaminants, including dyes, pharmaceuticals, pesticides, and agrochemicals, typically exhibit high chemical stability and strong bioaccumulation potential and thus represent a significant threat to ecological safety and public health globally,^[1–3] particularly given their resistance to traditional water remediation processes, which are reliant on chlorination.^[4–6] As such, there is a growing reliance on adsorption and filtration technologies to ensure removal from waste streams, with the fouled adsorbents, which require regular replacement, ultimately taken to landfill or incinerated, where pollutants may be released back into the wider environment, either directly, or as CO₂ in the latter scenario. Therefore, there is an urgent need for alternative remediation technologies.

Advanced oxidation processes (AOPs) have emerged as promising and sustainable solutions for effectively degrading persistent organic pollutants.^[7,8] Among the various AOPs, the utilization of Fenton-type systems (including those that combine pre-formed H₂O₂ with ozone (O₃/H₂O₂) or ultraviolet light (UV/H₂O₂)), has attracted substantial attention, owing to their capability to generate hydroxyl radicals (•OH), which offer high oxidative potential.^[9,10] However, practical and economic factors, primarily the high financial costs associated with reagents such as O₃ or H₂O₂ or indeed with high-energy light sources, have prevented implementation of these methods at scale.^[11] Similarly, the generation of •OH radicals from H₂O₂ via the use of Fenton(-type) reagents, typically homogenous species,^[12] has suffered from the need to remove active species from waste streams (often as Fe-rich sludge) and continually control pH to achieve optimal performance. Additionally, reliance on externally supplied commercial H₂O₂ elevates treatment costs,^[13] while the storage of highly concentrated H₂O₂ (typically shipped at concentrations in excess of 30 wt.%) poses considerable safety concerns.

The direct synthesis of H₂O₂ from molecular H₂ and O₂ represents an attractive alternative approach to producing H₂O₂ on-site,^[14] at concentrations required by the end-user, considerably lowering safety risks compared to those associated with handling industrially sourced H₂O₂, while also avoiding the presence of stabilizing agents (typically halides and acids), which are ubiquitously utilized to prolong the shelf life of commercial H₂O₂.^[15] Indeed, there is growing interest in the utilization of in situ generated H₂O₂ (and associated ROS) for oxidative chemical valorization.^[16–18] The application of such ROS, generated as reaction intermediates during H₂O₂ synthesis, has found further application in water disinfection, offering bactericidal and virucidal efficacy several orders of magnitude greater than that offered by preformed H₂O₂ or chlorination under equivalent conditions.^[19] However, despite their ability to generate

[a] R.-J. Li, R. J. Lewis, D. J. Morgan, G. J. Hutchings
Max Planck-Cardiff Centre on the Fundamentals of Heterogeneous Catalysis
FUNCAT, Cardiff Catalysis Institute, School of Chemistry, Cardiff University,
Translational Research Hub, Maindy Road, Cardiff CF24 4HQ, UK
E-mail: LewisR27@Cardiff.ac.uk
Hutch@Cardiff.ac.uk

[b] D. J. Morgan
HarwellXPS, Research Complex at Harwell (RCAH), Didcot OX11 0FA, UK

[c] E. Kitching, T. Slater
School of Chemistry, Cardiff Catalysis Institute, Cardiff University, Cardiff
CF24 4HQ, UK

Rong-Jian Li and Richard J. Lewis contributed equally to this work.

 Supporting information for this article is available on the WWW under
<https://doi.org/10.1002/cctc.202501264>


 © 2025 The Author(s). ChemCatChem published by Wiley-VCH GmbH. This is
an open access article under the terms of the [Creative Commons Attribution](https://creativecommons.org/licenses/by/4.0/)
License, which permits use, distribution and reproduction in any medium,
provided the original work is properly cited.

Table 1. The effect of Fe loading on the performance of 0.5%Au–0.5%Pd/TiO₂ catalysts toward the direct synthesis and subsequent degradation of H₂O₂.

Catalyst	H ₂ O ₂ Productivity (mol _{H2O2} kg _{cat} ^{−1} h ^{−1})	H ₂ O ₂ Conc. (ppm)	H ₂ Conv. (%)	H ₂ O ₂ Sel. (%)	H ₂ O ₂ Degradation (mol _{H2O2} kg _{cat} ^{−1} h ^{−1})
0.5%Au–0.5%Pd/TiO ₂	35	694	20	33	568
0.5%Au–0.5%Pd–0.1%Fe/TiO ₂	31	613	22	27	1022
0.5%Au–0.5%Pd–0.5%Fe/TiO ₂	31	611	23	26	853
0.5%Au–0.5%Pd–1%Fe/TiO ₂	7	132	26	5	780
0.5%Au–0.5%Pd–2%Fe/TiO ₂	2	33	30	1	589
0.5%Au–0.5%Pd–3%Fe/TiO ₂	2	31	30	1	540
0.5%Au–2%Fe/TiO ₂	0	2	N.D	N.D	32
0.5%Pd–2%Fe/TiO ₂	7	148	33	4	288
0.5%Au/TiO ₂	0	13	2	8	24
0.5%Pd/TiO ₂	29	582	21	26	580
2%Fe/TiO ₂	0	0	0	0	56

H₂O₂ direct synthesis reaction conditions: catalyst (0.01 g), H₂O (8.5 g), 5% H₂/CO₂ (420 psi), 25% O₂/CO₂ (160 psi), 0.5 h, 20 °C, 1200 rpm. **H₂O₂ degradation reaction conditions:** catalyst (0.01 g), H₂O₂ (50 wt% 0.68 g), H₂O (7.82 g), 5% H₂/CO₂ (420 psi), 0.5 h, 20 °C, 1200 rpm. N.D: unable to determine due to limits of detection.

ROS, these systems, which are based on supported AuPd catalysts, have so far offered only a limited reactivity towards the remediation of organic pollutants.^[20] Building on these studies, the coupling of Pd, responsible for H₂O₂ synthesis, with Fenton(-type) metals responsible for ROS generation has been investigated for pollutant remediation,^[21] and while such formulations offer improved activity compared to their bimetallic AuPd counterparts, they still typically suffer from limited reactivity.

With these studies in mind, and building on the extensive H₂O₂ direct synthesis literature, which outlines the synergistic effects that may be achieved from the alloying of Pd with Au,^[22–24] we now investigate the efficacy of trimetallic AuPdFe-based catalysts that combine the direct H₂O₂ synthesis activity of AuPd nanoalloys with the ability of Fe to generate ROS via Fenton's pathways for the remediation of phenol, with a proposed reaction schematic for the oxidative degradation of this model recalcitrant reported in Figure S1.

2. Results and Discussion

Under reaction conditions considered sub-optimal for H₂O₂ production (i.e., ambient temperature^[25] and in the absence of the alcohol co-solvent typically utilized to promote H₂O₂ stability and gaseous reagent solubility), but relevant to the real-world oxidative treatment of aqueous waste streams, our initial studies evaluated catalytic performance of a series of TiO₂-immobilized AuPdFe catalysts (with AuPd content fixed at 1 wt.% and Au/Pd = 1 (wt/wt)) toward the direct H₂O₂ synthesis and subsequent degradation of H₂O₂ (Table 1, with further detailed evaluation of key catalytic formulations over extended reaction time reported in Figure S2). In keeping with earlier works,^[26–28] the incorporation of Au into a supported Pd catalyst was found to improve catalytic activity toward H₂O₂ production, with H₂O₂ synthesis rates (35 mol_{H2O2} kg_{cat}^{−1} h^{−1}), observed over the bimetallic catalyst somewhat greater than that offered

by the Pd-only catalyst with an equivalent Pd content (29 mol_{H2O2} kg_{cat}^{−1} h^{−1}). Notably, this improved performance can be related to enhancements in catalytic selectivity, rather than increased reactivity, as indicated by the near-identical H₂ conversion rates observed over these formulations (33% and 26% H₂O₂ selectivity for the 0.5%Au–0.5%Pd/TiO₂ and 0.5%Pd/TiO₂ catalysts, respectively, at approx. 20% H₂ conversion). For a comprehensive overview of the role of Au in promoting catalytic performance toward the direct synthesis of H₂O₂ and an in-depth discussion of the H₂O₂ direct synthesis mechanism, the reader is directed to the seminal works from the Yoshizawa and Flaherty laboratories.^[23,27,29]

We have previously reported that the incorporation of tertiary base metals, including Fe, into AuPd nanoalloys can result in a considerable improvement in H₂O₂ synthesis rates, with this enhancement a result of the electronic modification of Pd through the formation of trimetallic nanoalloys.^[30,31] Our analysis of the as-prepared AuPdFe formulations by CO-DRIFTS (Figure S3 and associated text) and XPS (Figure S4 and associated text) aligns well with these earlier studies and reveals that the introduction of Fe can indeed result in a modification of Pd speciation, with no considerable variation in mean nanoparticle size observed across the catalytic series (Figures S5 and S6 and Table 2). However, under our chosen reaction conditions, we do not observe the promotive effect on H₂O₂ synthesis activity previously reported to result from the formation of AuPdFe nanoalloys.^[30] While such discrepancies may be attributed to the use of reaction conditions considered far more favorable toward H₂O₂ stability in these earlier works (i.e., sub-ambient temperatures and an alcohol co-solvent), it is important to note that the Fe-content of the catalysts investigated in this study are significantly higher than those formulations found to be optimal for H₂O₂ synthesis in our previous investigations, where a considerable promotive effect was observed upon the addition of dopant concentrations of Fe (in the range of 2%–5% of the total metal loading). Indeed, we have previously identified that out-

Table 2. Mean particle size of key AuPdFe/TiO₂ catalysts, as determined by TEM analysis.

Catalyst	Mean Particle size (nm)	Standard Deviation (nm)
0.5%Au-0.5%Pd/TiO ₂	4.4	1.7
0.5%Au-0.5%Pd-0.1%Fe/TiO ₂	3.9	2.1
0.5%Au-0.5%Pd-0.5%Fe/TiO ₂	3.2	1.2
0.5%Au-0.5%Pd-1%Fe/TiO ₂	3.7	1.9
0.5%Au-0.5%Pd-2%Fe/TiO ₂	4.9	2.1
0.5%Au-0.5%Pd-3%Fe/TiO ₂	6.1	2.7

Note: catalysts exposed to a reductive heat treatment prior to analysis (5% H₂/Ar, 400 °C, 4 h, 10 °C min⁻¹).

side this narrow concentration range, the introduction of tertiary metal dopants may result in a considerable loss in catalytic activity toward H₂O₂ production.^[32] In this context, it is, therefore, perhaps unsurprising that the incorporation of Fe, especially at higher loadings, into the bimetallic 0.5%Au-0.5%Pd/TiO₂ formulation was found to result in a deleterious effect on H₂O₂ synthesis rates. Notably, this loss of performance, particularly observed at higher Fe loadings, can be associated with a decrease in catalytic selectivity toward H₂O₂, which aligns well with our earlier studies into alternative, non-Fe-containing trimetallic formulations.^[31,32]

The use of heterogeneous Fe species to catalyze the formation of reactive oxygen species (ROS, including •OOH, •OH, and •O₂⁻) from preformed and in situ generated H₂O₂ for use in chemical valorization and pollutant remediation is an area of growing interest, and indeed we have recently demonstrated that the combination of Pd with Fenton's-type metals represents an attractive route for the oxidative degradation of organic contaminants.^[33] However, the extent to which the high cost of preformed H₂O₂, and the presence of proprietary stabilizing agents used to prolong H₂O₂ shelf life, would preclude application in pollutant remediation should be considered. With these earlier works in mind, and building on our initial studies, we next evaluated efficacy of these AuPdFe-based catalysts toward the oxidative degradation of phenol via the in situ production of H₂O₂ and associated reactive oxygen species (Figure 1, with additional data reported in Figure S7). We note that it was not possible to measure residual H₂O₂ via standard titration or colorimetric procedures given the strong reddish color that results from the formation of the aromatic oxidation products (catechol, hydroquinone, etc.), generated as a result of phenol oxidation. A stark divide in catalyst performance was observed, with the Fe-rich (>1 wt% Fe) catalysts offering significantly higher rates of phenol conversion than the lower Fe-loaded analogues. Notably, this is despite the higher rates of H₂O₂ synthesis observed over the Fe-lean formulations (Table 1), which suggests that H₂O₂ itself may not be the primary reactive oxygen species responsible for the observed catalysis. Rather, this observation implicates the role of the oxygen-based radical species generated via Fenton's pathways from H₂O₂, as the key driver of oxidative degradation. Regardless, the relatively high selectivity of all catalysts stud-

ied, towards the highly oxidized products (i.e., oxalic, maleic, and fumaric acids, etc.), rather than the phenolic derivatives (catechol, resorcinol, etc.), is highly promising given the significant health risks posed by partially oxidized phenolic intermediates, which are typically considered more harmful than phenol itself.

Investigation of the AuPd/Fe ratio identified the 0.5%Au-0.5%Pd-2%Fe/TiO₂ catalyst as the optimal formulation, achieving phenol conversion rates (83% at a reaction time of 6 h) in excess of ten times that offered by the bimetallic AuPd-based parent material (8% at a reaction time of 6 h) and far greater than that offered by the bimetallic 0.5%Pd-2%Fe/TiO₂ catalyst (58% at a reaction time of 6 h), highlighting the key role of Au (Figure 1, with additional data reported in Figure S8). The reader is directed to Table S1, which proved a comparison of catalytic performance of the key formulations reported in this work with that of alternative formulations reported in the literature.

Notably, in the case of the trimetallic series, phenol degradation activity was observed to decrease with the introduction of Fe in excess of 2 wt%. The performance of the optimal 0.5%Au-0.5%Pd-2%Fe/TiO₂ catalyst is particularly noteworthy given the relatively high selective utilization of H₂ offered by this material (21% H₂ conversion at a reaction time of 6 h), with poor H₂ efficiency a longstanding hurdle for numerous processes that seek to utilize the in situ approach, particularly for chemical synthesis.^[34] Furthermore, based on a comparison of catalytic performance toward individual reaction pathways (i.e., H₂O₂ direct synthesis and the oxidative degradation of phenol, Table 1 and Figure 1, respectively), it is clear that H₂O₂ synthesis activity is not a strong indicator for catalytic performance in the in situ cascade, which further supports our hypothesis that H₂O₂ itself is not the key oxidative species responsible for phenol oxidation. Indeed, based on this metric alone, one would not have expected the 0.5%Au-0.5%Pd-2%Fe/TiO₂ catalyst to offer any reasonable activity towards the degradation of phenol.

Notably, while the 0.5%Au-0.5%Pd-2%Fe/TiO₂ catalyst offered reasonably high selectivities toward the highly oxidized products (i.e., the acids), a considerable proportion of hydroquinone and catechol was still observed in post-reaction product streams, even at extended reaction times (15% and 21% selectivity toward hydroquinone and catechol, respectively, at a reaction time of 6 h). Such data correlates well with our investigations into the efficacy of the in situ route to the oxidative degradation of the various phenolic derivatives (Figure S9) and indicates the relative variation in the efficacy of reactive oxygen species towards the degradation of the various phenolic derivatives.

Subsequent studies established the requirement for the active metals to be immobilized on the same support grain, with the activity of the 0.5%Au-0.5%Pd-2%Fe/TiO₂ catalyst (83% phenol conversion) far superior to that of a physical mixture of the 0.5%Au-0.5%Pd/TiO₂ and 2%Fe/TiO₂ catalysts (22% phenol conversion) when using an identical metal concentration to that used in the optimal trimetallic analogue (Figure S10). The observation of phenolic degradation in the absence of Fenton's active metals (i.e., over the bimetallic AuPd catalyst) is indeed interesting, and when considered alongside earlier works that have reported the ability of Au to promote the release of ROS from Pd-based surfaces,^[17,19,23] may imply multiple routes to ROS

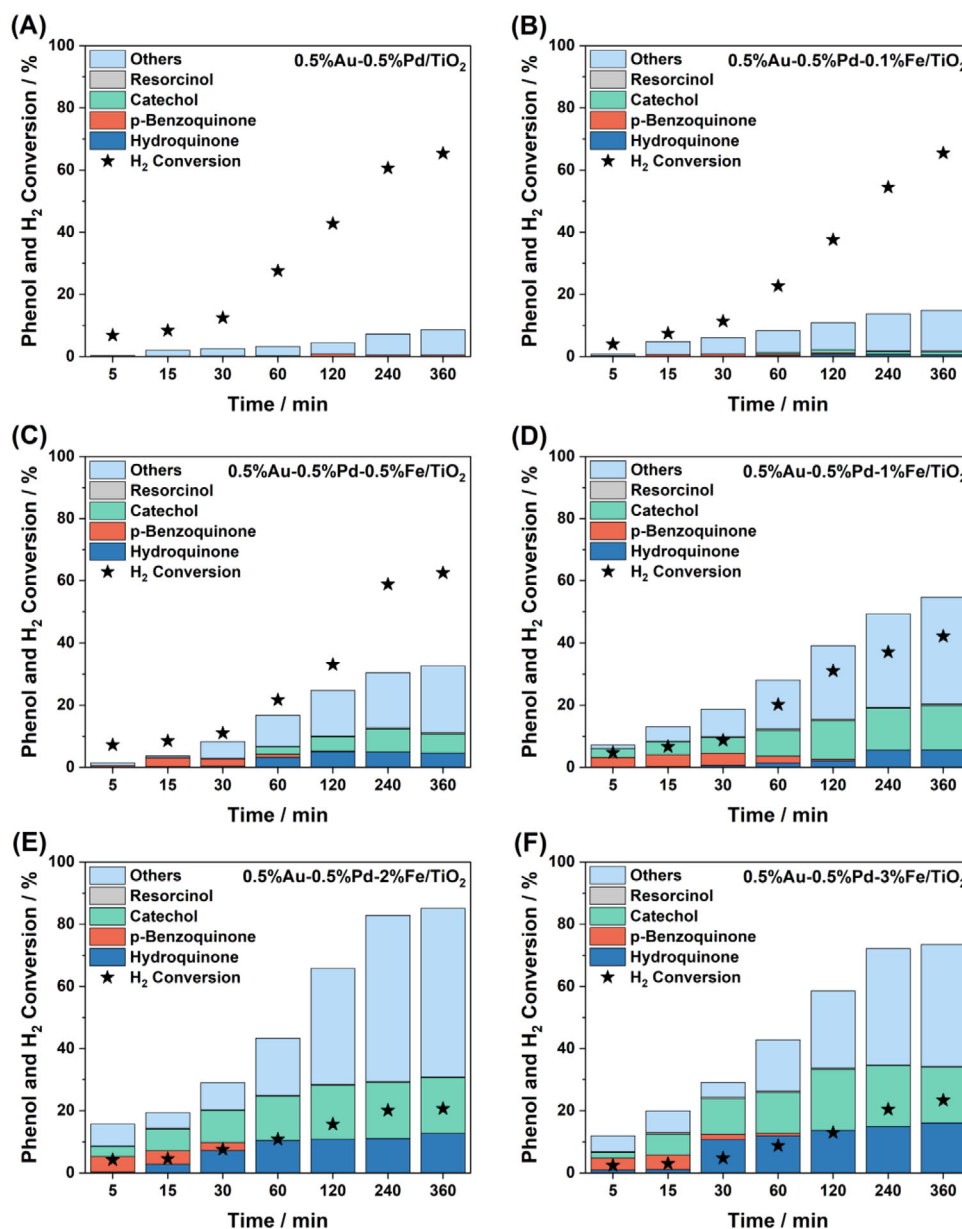


Figure 1. Catalytic activity of AuPdFe/TiO₂ catalysts toward the oxidative degradation of phenol, via in situ H₂O₂ production, as a function of AuPd/Fe ratio. Phenol degradation reaction conditions: catalyst (0.01 g), phenol (1000 ppm, 8.5 g), 5% H₂/CO₂ (420 psi), 25% O₂/CO₂ (160 psi), 20 °C, 1200 rpm.

generation. Namely, it is hypothesized that these highly potent oxidizing species are generated primarily as reaction intermediates formed during H₂O₂ synthesis over AuPd surfaces, while Fenton-type pathways are considered to be the dominant route to their formation upon Fe incorporation. A significant improvement in phenol conversion was observed in the presence of both H₂ and O₂ (i.e., under in situ conditions), in comparison to that observed when using either molecular H₂ (3% phenol conversion) or O₂ (1% phenol conversion) or indeed in the presence of pre-formed H₂O₂ (4% phenol conversion with H₂O₂ alone and 14% phenol conversion in the presence of catalyst and H₂O₂, when utilizing a H₂O₂ concentration equivalent to that which may be achieved if all the H₂ in the in situ system was selectively converted to H₂O₂) (Figure S11). Crucially, these latter experiments further implicate the highly reactive oxygen-

based radical species other than H₂O₂ as primarily responsible for the observed activity. Further, support for the key role of ROS, rather than H₂O₂, in the oxidative degradation of phenol is provided from radical quenching experiments (Figure S12), where a substantial decrease in phenol conversion was observed in the presence of *t*-butanol, a widely utilized scavenger for O-based radical species.^[35]

Returning to our investigation into catalyst performance over extended reaction times and with a focus on the 0.5%Au-0.5%Pd-2%Fe/TiO₂ catalyst, ICP-MS analysis of post-reaction solutions revealed the relative stability of both Au and Pd (Table S2). However, a significant proportion of leached Fe was observed, with the extent of Fe loss correlating well with the extent of phenol conversion (Figure S13), which may be indicative of product-mediated leaching. Indeed, further experiments under

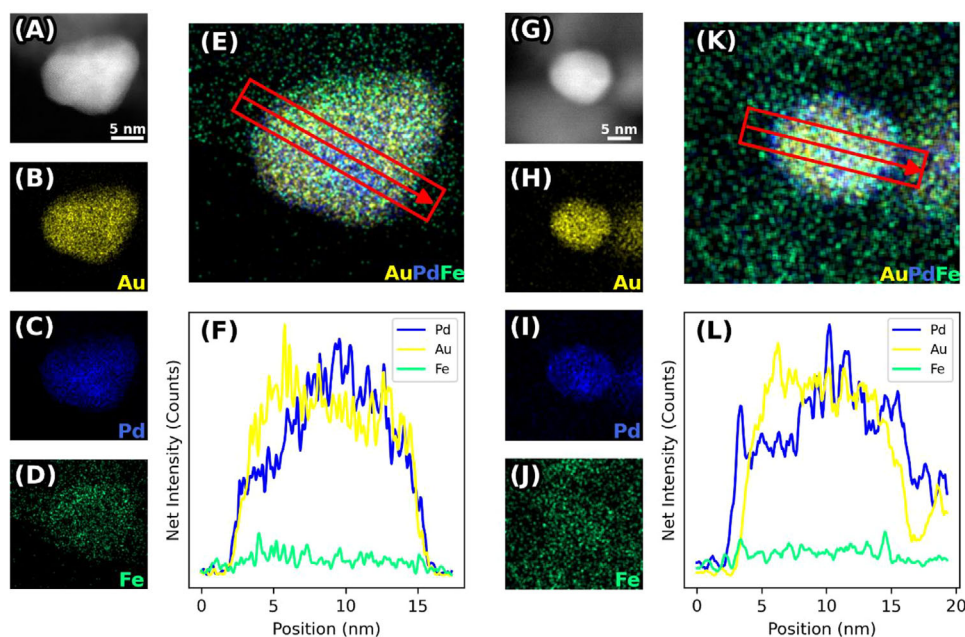


Figure 2. Representative HAADF-STEM images and complementary EDX analysis of individual alloy nanoparticles in a)–f) fresh and g)–l) used 0.5%Au-0.5%Pd-2%Fe/TiO₂ catalyst. Phenol degradation reaction conditions: catalyst (0.01 g), phenol (1000 ppm, 8.5 g), 5% H₂/CO₂ (420 psi), 25% O₂/CO₂ (160 psi), 20 °C, 4 h, 1200 rpm. Note: The fresh catalyst was exposed to a reductive heat treatment prior to use (5%H₂/Ar, 400 °C, 4 h, 10 °C min^{−1}). The used sample was dried (30 °C, under vacuum, 16 h) prior to analysis.

ambient conditions confirm the role of the highly oxidized products (particularly formic, oxalic, and manolic acids), in promoting catalyst deactivation (Table S3). Such observations are in keeping with previous investigations that established the ability of phenolic oxidative products to chelate to heterogeneous Fe species and promote their dissolution. Further investigation into catalyst stability through reuse experiments (Figure S14) revealed a near 50% loss in catalytic performance upon second use and clearly suggests that further catalyst and process design is necessary in order to achieve optimal catalyst performance and stability. Interestingly, while phenolic degradation activity decreases sharply upon reuse, H₂ conversion rates were found to increase considerably from 20% to 48%, which aligns well with our evaluation of catalytic performance towards H₂O₂ synthesis activity after exposure to phenolic degradation conditions (Figure S15). Such observations align well with the observed stability of the H₂O₂ synthesizing component (i.e., Au and Pd) (Table S2) and the observed shift of Pd oxidation state towards Pd⁰ (Figure S16), which is well known to offer improved H₂O₂ synthesis activity compared to Pd²⁺ analogues.^[36]

HAADF-STEM and corresponding EDX analysis of the as-prepared and used 0.5%Au-0.5%Pd-2%Fe/TiO₂ catalyst are presented in Figure 2 (with additional data reported in Figures S17–S22). Notably, the extent of intimate incorporation of Fe into the AuPd nanoalloys was limited, with considerable quantities of unalloyed Fe found in addition to AuPd-rich, Fe-lean, trimetallic alloys. Aligning well with the stability of the AuPd component indicated by ICP-MS, we do not observe a meaningful change in particle size upon exposure of the catalyst to phenolic degradation conditions. However, we do observe a limited number of particles in the post-reaction sample that have a clear Pd-

rich shell and Au-rich core morphology (Figure S22), indicating segregation of Pd to the surface of nanoparticles.

With a continued focus on the 0.5%Au-0.5%Pd-2%Fe/TiO₂ catalyst, we subsequently conducted a series of hot-filtration experiments to identify the contribution of leached metal species to catalytic activity (Figure 3). In the absence of the solid catalyst, minimal additional phenol conversion was observed (69%) after a two-part, 4 h experiment. This value was nearly identical to that observed for the 0.5%Au-0.5%Pd-2%Fe/TiO₂ catalyst over a 2 h reaction (66%), with the limited additional conversion of phenol possibly attributed to the contribution from residual H₂O₂ generated in the initial 2 h reaction. To determine if the inactivity observed in the 0.5%Au-0.5%Pd-2%Fe/TiO₂ hot-filtration experiment was due to the limited ability of any potential homogeneous component to synthesize H₂O₂ (which would align well with our earlier observation of AuPd stability, Table S2, Figure 2), a further hot-filtration experiment was conducted whereby, after the initial 2 h reaction, the 0.5%Au-0.5%Pd-2%Fe/TiO₂ catalyst was replaced with the 0.5%Au-0.5%Pd/TiO₂ analogue, ensuring that the total moles of Au and Pd were equal to that in the 0.5%Au-0.5%Pd-2%Fe/TiO₂ formulation. Perhaps unexpectedly, given the activity of the 0.5%Au-0.5%Pd/TiO₂ catalyst toward the oxidative degradation of phenol (Figure 1) an increase in this metric was observed (75%), comparable to the sum of the 0.5%Au-0.5%Pd-2%Fe/TiO₂ (66%) and 0.5%Au-0.5%Pd/TiO₂ (4%) components when used independently over 2 h. Given the ability of the 0.5%Au-0.5%Pd/TiO₂ catalyst to promote the degradation of phenol, this experiment was unable to fully confirm a contribution from homogeneous species. In a final experiment, after the initial 2 h reaction utilizing the 0.5%Au-0.5%Pd-2%Fe/TiO₂ catalyst alone, commercial H₂O₂, at a

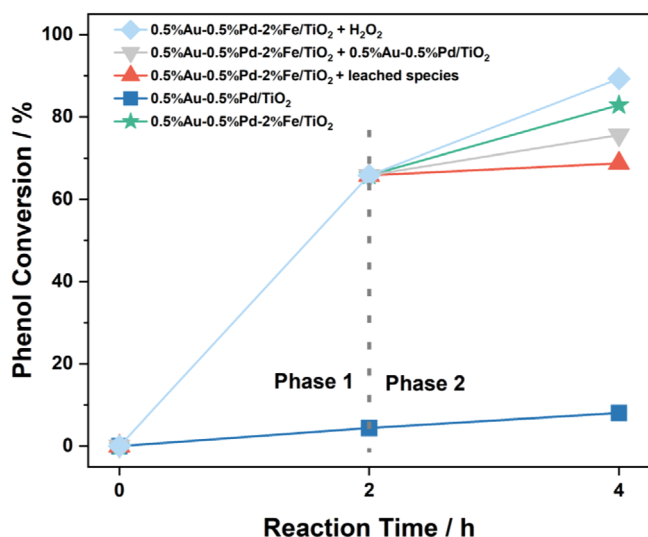


Figure 3. The contribution of leached species in the oxidative degradation of phenol, as identified by hot filtration experiments. Phenol oxidation reaction conditions: catalyst (0.01 g), phenol (8.5 g, 1000 ppm), 5% H₂/CO₂ (420 psi), 25% O₂/CO₂ (160 psi), 1200 rpm, 20 °C, 1200 rpm. Key: 1%AuPd-2%Fe/TiO₂ catalyzed reaction (green star); 0.5%Au-0.5%Pd/TiO₂ catalyzed reaction (blue square); hot filtration reaction where the 0.5%Au-0.5%Pd-2%Fe/TiO₂ catalyst is removed by filtration after 2 h (red triangles); hot filtration reaction where 0.5%Au-0.5%Pd-2%Fe/TiO₂ catalyst removed by filtration after 2 h and replaced by 0.5%Au-0.5%Pd/TiO₂ catalyst for final 2 h of reaction (grey inverted triangles); hot filtration reaction where 0.5%Au-0.5%Pd-2%Fe/TiO₂ catalyst is removed by filtration after 2 h and replaced by commercial H₂O₂ (at a concentration identical to that if all H₂ utilized in a standard in-situ reaction was selectively converted to H₂O₂) for the final 2 h of reaction (blue diamonds).

concentration equivalent to if all H₂ in a standard phenol degradation reaction was selectively converted to H₂O₂, was added to the reaction mixture. After a further 2 h of reaction (carried out in the presence of an atmosphere of CO₂), a significant increase in phenol conversion was observed (89%), which, when considered alongside our observations of negligible phenol degradation in the presence of H₂O₂ alone (Figure S11), indicates the contribution of leached metals to the observed catalytic performance. Indeed, such observations align well with additional studies focused on the combination of a heterogeneous 0.5%Au-0.5%Pd/TiO₂ catalyst and homogenous Fe species (Figure S22), which demonstrate a considerable increase in phenol degradation activity upon the introduction of the homogeneous component.

3. Conclusion

We have demonstrated that the incorporation of Fe into supported AuPd nanoalloys can offer enhanced catalytic performance towards the oxidative degradation of phenol via in situ production of H₂O₂ and associated reactive oxygen species, compared to the parent bimetallic formulation, with the activity of the optimal 0.5%Au-0.5%Pd-2%Fe/TiO₂ catalyst approximately 10 times greater than that offered by the AuPd-analogue. Here it is important to note that identifying the origin of these ROS is particularly challenging, given the potential for them to form

through direct combination of O₂ and H₂ over Pd-based surfaces or through the successive degradation of formed H₂O₂ via Fe-mediated pathways.

Catalyst stability was found to be a considerable concern, with substantial leaching of Fe observed, mainly promoted by the formation of deeply oxidized products (primarily formic, oxalic, and muconic acids). While we consider that these catalysts represent a promising basis for further exploration for the oxidative degradation of a range of recalcitrants. However, it is clear that additional efforts are required to 1) fully understand the origin and contribution of individual reactive oxygen species to the observed catalysis, 2) gain insight into the mechanism by which phenolic degradation products promote the leaching of active metals, and 3) evaluate the dynamic nature of metal species under exposure to reaction conditions via a range of operando techniques to inform future improvements in catalyst design.

4. Experimental Section

4.1. Catalyst Synthesis

A series of mono-, bi-, and tri-metallic 0.5%Au-0.5%Pd-X%Fe/TiO₂ (X = 0–3) catalysts have been prepared by a wet co-impregnation procedure, based on a methodology previously reported in the literature.^[29] The procedure to produce 0.5%Au-0.5%Pd-2%Fe/TiO₂ (1 g) is outlined below. In all cases the combined loading of the precious metals is 1 wt% and the Au/Pd ratio is 1:1 (wt/wt).

Aqueous solutions of HAuCl₄·3H₂O (0.403 mL, [Au] = 12.4 mg mL⁻¹, Strem Chemicals), PdCl₂ (0.586 mL, [Pd] = 8.5 mg mL⁻¹, Sigma-Aldrich) and FeCl₃ (4.032 mL, [Fe] = 4.96 mg mL⁻¹, Sigma Aldrich) were mixed in a 50 mL round-bottom flask and heated to 65 °C with stirring (1000 rpm) in a thermostatically controlled oil bath, with total volume fixed to 16 mL using H₂O (HPLC grade, Fischer Scientific). Upon reaching 65 °C, TiO₂ (0.97 g, P25, Degussa) was added over 10 min with constant stirring. The resulting slurry was stirred at 65 °C for a further 15 min; following this, the temperature was raised to 85 °C for 16 h to allow for complete evaporation of water. The resulting solid was ground before heat treatment in a reductive atmosphere (5%H₂/Ar, 400 °C, 4 h, 10 °C min⁻¹).

4.2. Catalyst Testing

Note 1: Reaction conditions used within this study operate under the flammability limits of gaseous mixtures of H₂ and O₂.

4.3. Direct Synthesis of H₂O₂

Hydrogen peroxide synthesis was evaluated using a Parr Instruments stainless steel autoclave with a nominal volume of 50 mL, equipped with a PTFE liner so that the total volume is reduced to 33 mL, and a maximum working pressure of 2000 psi. The autoclave liner was charged with catalyst (0.01 g) and H₂O (8.5 g, HPLC grade, Fischer Scientific). The charged autoclave was then purged three times with 5%H₂/CO₂ (100 psi) before filling with 5%H₂/CO₂ to a pressure of 420 psi, followed by the addition of 25%O₂/CO₂ (160 psi), with the pressure of 5%H₂/CO₂ and 25%O₂/CO₂ given as gauge pressures. The reactor was not continually fed with reactant gas. The reaction was conducted at room temperature of 20 °C for 0.5 h with

stirring (1200 rpm). It should be noted that individual experiments were carried out, and the reactant mixture was not sampled on line.

To determine net H_2O_2 concentration, the solid catalyst was removed via filtration, and an aliquot (2.0 mL) of the post-reaction solution was combined with potassium titanium oxalate dihydrate solution acidified with 30% H_2SO_4 (0.02 M, 2.0 mL), resulting in the formation of an orange perititanic acid complex. This resulting solution was analyzed spectrophotometrically using an Agilent Cary 60 UV/Vis Spectrophotometer at 400 nm by comparison to a calibration curve. Catalyst productivities are reported as $\text{mol}_{\text{H}_2\text{O}_2} \text{kg}_{\text{cat}}^{-1} \text{h}^{-1}$.

The catalytic conversion of H_2 and selectivity toward H_2O_2 were determined using a Varian 3800 GC fitted with TCD and equipped with a Porapak Q column.

H_2 conversion (Equation 1) and H_2O_2 selectivity (Equation 2) are defined as follows:

$$\text{H}_2 \text{ Conversion (\%)} = \frac{\text{mmol}_{\text{H}_2(t(0))} - \text{mmol}_{\text{H}_2(t(1))}}{\text{mmol}_{\text{H}_2(t(0))}} \times 100 \quad (1)$$

$$\text{H}_2\text{O}_2 \text{ Selectivity (\%)} = \frac{\text{H}_2\text{O}_2 \text{ detected (mmol)}}{\text{H}_2 \text{ consumed (mmol)}} \times 100 \quad (2)$$

The total autoclave capacity was determined via water displacement to allow for the accurate determination of H_2 conversion and H_2O_2 selectivity. When equipped with the PTFE liner, the total volume of an unfilled autoclave was determined to be 33 mL, which includes all available gaseous space within the autoclave.

4.4. Degradation of H_2O_2

Catalytic activity toward H_2O_2 degradation was determined in a similar manner to the direct synthesis activity of a catalyst. The autoclave liner was charged with solvent H_2O (7.82 g, HPLC grade, Fischer Scientific) and H_2O_2 (50 wt%, 0.68 g, Sigma Aldrich), with the solvent composition equivalent to a 4 wt% H_2O_2 solution. From the solution, two 0.05 g aliquots were removed and titrated with an acidified $\text{Ce}(\text{SO}_4)_2$ solution using ferroin as an indicator to determine an accurate concentration of H_2O_2 at the start of the reaction. Subsequently, the catalyst (0.01 g) was added to the reaction media, and the autoclave was purged with 5% H_2/CO_2 (100 psi) before being pressurized with 5% H_2/CO_2 (420 psi). The reaction medium was conducted at a temperature of 20 °C, and stirred (1200 rpm) for the desired reaction time. After the reaction was complete, the catalyst was removed from the reaction mixture, and two 0.05 g aliquots were titrated against the acidified $\text{Ce}(\text{SO}_4)_2$ solution using ferroin as an indicator. The degradation activity is reported as $\text{mol}_{\text{H}_2\text{O}_2} \text{kg}_{\text{cat}}^{-1} \text{h}^{-1}$.

In all cases, reactions were run three times over multiple batches of catalyst for the optimal formulation, with the data being presented as an average of these experiments. The catalytic activity toward the direct synthesis and subsequent degradation of H_2O_2 was found to be consistent to within $\pm 2\%$ on the basis of multiple reactions.

4.5. Phenol Degradation via the In Situ Synthesis of H_2O_2

Catalytic activity toward the degradation of phenol was evaluated using a Parr Instruments stainless steel autoclave with a nominal volume of 50 mL, equipped with a glass liner so that nominal volume is reduced to 33 mL, and a maximum working pressure of 2000 psi. In a typical test the autoclave was charged with catalyst (0.01 g) and aqueous phenol (8.5 g, 1000 ppm). The charged autoclave was then purged three times with 5% H_2/CO_2 (100 psi)

before filling with 5% H_2/CO_2 to a pressure of 420 psi, followed by the addition of 25% O_2/CO_2 (160 psi). The pressure of 5% H_2/CO_2 and 25% O_2/CO_2 are given as gauge pressures. Reactant gases were not continually supplied. The reactor was then heated to 20 °C followed by stirring (1200 rpm), typically for 4 h. After 4 h gas mixtures were sampled and analyzed via GC (Varian 3800 GC fitted with a TCD and equipped with a Porapak Q column). The catalyst was removed from the reaction solution via filtration, and the post-reaction solution was subsequently analyzed using high-performance liquid chromatography (HPLC) fitted with an Agilent Poroshell 120 SB-C18 column.

Throughout this study, phenol oxidation product distribution has been grouped into two categories, namely the phenolic derivatives (catechol, hydroquinone, resorcinol, and benzoquinone) and others, which include the organic acids (formic acid, acetic acid, fumaric acid, maleic acid, malonic acid, muconic acid, and oxalic acid), water, and carbon dioxide (i.e., the products of total oxidation). Note that while it is possible for the completed oxidation of phenol to occur, the presence of water as a reaction medium and carbon dioxide as a reagent gas diluent prevents the detection of these products.

Phenol conversion (Equation 3), selectivity toward phenolic derivatives (PD) (Equation 4) or others (organic acids, CO_2 , and H_2O) (Equation 5) are defined as follows:

$$\text{Phenol Conversion (\%)} = \frac{\text{mmol}_{\text{Phenol}(t(0))} - \text{mmol}_{\text{Phenol}(t(1))}}{\text{mmol}_{\text{Phenol}(t(0))}} \times 100 \quad (3)$$

$$\text{Selectivity towards PD (\%)} = \frac{\text{mmol}_{\text{PD}}}{\text{mmol}_{\text{phenol converted}}} \times 100 \quad (4)$$

$$\text{Selectivity towards others (\%)} = \frac{\text{mmol}_{\text{phenol}(t(1))} - \text{mmol}_{\text{PD}(t(1))}}{\text{mmol}_{\text{phenol}(t(1))}} \times 100 \quad (5)$$

Comparative phenol degradation experiments were conducted using commercial H_2O_2 (50 wt%, Merck), at a concentration equal to that produced if all H_2 in a standard in situ reaction was selectively converted to H_2O_2 .

To probe the contribution of alternative pathways to phenol conversion (i.e., via aerobic or reductive pathways), an identical procedure to that outlined above for the oxidative degradation of phenol was followed, with the reactor charged with 5% H_2/CO_2 (420 psi) or 25% O_2/CO_2 (160 psi) reagent gases; total pressure was maintained at 580 psi using CO_2 .

In all cases, reactions were run three times over multiple batches of catalyst for the optimal formulation, with the data being presented as an average of these experiments. Catalytic activity toward the oxidative degradation of phenol was found to be consistent to within $\pm 4\%$ on the basis of multiple reactions.

4.6. Hot Filtration Experiments for In Situ Phenol Degradation

An identical procedure to that outlined above for the oxidative degradation of phenol was followed for a reaction time of 2 h. Following this, the stirring was stopped, and the reactant gas mixture was vented prior to the removal of the solid catalyst via filtration. The post-reaction solution was returned to the reactor, reagent

gases were reintroduced, and the reaction was allowed to run for a further 2 h to identify the contribution of leached species to the observed activity. Further experiments were conducted, where fresh 1% AuPd/TiO₂ catalyst (0.01 g) or preformed H₂O₂ (1.93 mmol), comparable to that if all the H₂ converted in the first 2 h reaction was converted selectively to H₂O₂, was added to the reaction mixture prior to running the reaction for a further 2 h.

4.7. Catalyst Characterization

X-ray photoelectron spectroscopy (XPS) measurements were performed on a Kratos Axis Ultra-DLD photoelectron spectrometer utilizing a monochromatic Al K_α X-ray source operating at 144 W (12 mA × 12 kV). Samples were pressed onto silicone-free double-sized Scotch tape and analyzed using the hybrid spectroscopy mode, giving an analysis area of ca. 700 × 300 microns. High-resolution and survey spectra were acquired at pass energies of 40 eV (step size 0.1 eV) and 160 eV (step size 1 eV), respectively. Charge compensation was performed using low-energy electrons, and the resulting spectrum was calibrated to the lowest C(1s) peak from the fitted carbon core-level spectra, taken to be 284.8 eV. The suitability of the C(1s) referencing was confirmed by a secondary reference point, taken to be the Ti(2p_{3/2}) peak with a binding energy of 458.7 eV, characteristic of that for virgin TiO₂. All data were processed using CasaXPS v2.3.24 using a Shirley background and modified Wagner factors as supplied by the instrument manufacturer. Peak fits were performed using a combination of Voigt-type functions (LA line shape in CasaXPS) and models derived from bulk reference samples where appropriate.

The bulk structure of the catalysts was determined by powder X-ray diffraction using a (θ–θ) PANalytical X'pert Pro powder diffractometer using a Cu K_α radiation source, operating at 40 keV and 40 mA. Analysis was carried out using between 2θ values of 20°–80°.

Note 2: X-ray diffractograms of the as-prepared catalysts are reported in Figures S23 and S24, with no reflections associated with active metals, indicative of the relatively low total loading and high dispersion of the immobilized metals.

Transmission electron microscopy (TEM) was performed on a JEOL JEM-2100 operating at 200 kV. Samples were prepared by dispersion in ethanol by sonication and deposited on 300-mesh copper grids coated with holey carbon film. To allow for the determination of mean particle size, a minimum of 300 particles were measured. Aberration-corrected scanning transmission electron microscopy (AC-STEM) was performed using a probe-corrected ThermoFisher Spectra 200 S/TEM operating at 200 kV and a convergence semi-angle of 29.5 mrad. High spatial resolution STEM imaging was acquired with a high-angle annular dark field (HAADF) detector an inner collection angle of approximately 56 mrad (outer angle of approximately 200 mrad). Energy dispersive X-ray spectroscopy (EDX) was performed using a ThermoFisher Super-X detector, and the data was analyzed using Thermo Scientific Velox Software. CO-DRIFTS measurements were taken on a Bruker Tensor 27 spectrometer fitted with a mercury cadmium telluride (MCT) detector. The sample was loaded into the Praying Mantis high temperature (HVC-DRP-4) in-situ cell before exposure to N₂ and then 1% CO/N₂ at a flow rate of 50 cm³ min^{−1}. A background spectrum was obtained using KBr, and measurements were recorded every 1 min at room temperature. Once the CO adsorption bands in the DRIFT spectra ceased to increase in intensity, the gas feed was changed back to N₂ in order to evacuate gaseous CO. Measurements were repeated until no change in subsequent spectra was observed.

Total metal leaching from the supported catalyst under in situ phenol degradation conditions, or under model leaching conditions, where the catalyst was exposed to phenolic degradation products

(1000 ppm, 0.5 h, 1200 rpm under ambient conditions), was quantified via inductively coupled plasma mass spectrometry (ICP-MS). Post-reaction solutions were analyzed using an Agilent 7900 ICP-MS equipped with I-AS auto-sampler. All samples were diluted by a factor of 10 using HPLC grade H₂O (1% HNO₃ and 0.5% HCl matrix). All calibrants were matrix-matched and measured against a five-point calibration using certified reference materials purchased from Perkin Elmer and certified internal standards acquired from Agilent.

To allow for the quantification of total metal loading, catalysts were digested via an aqua-regia-assisted microwave digestion method using a Milestone Connect Ethos UP microwave with an SK15 sample rotor. Digested samples were analyzed by inductively coupled plasma–optical emission spectroscopy (ICP-MS). All calibrants were matrix-matched and measured against a five-point calibration using certified reference materials purchased from Perkin Elmer and certified internal standards acquired from Agilent. Actual metal loadings of key catalytic samples are provided in Table S4.

Brunauer–Emmett–Teller (BET) surface area measurements were conducted using a Quadrasorb surface area analyzer. A 5-point isotherm of each material was measured using N₂ as the adsorbate gas. Samples were degassed at 250 °C for 2 h prior to the surface area being determined by 5-point N₂ adsorption at −196 °C, and data were analyzed using the BET method. Surface area measurements of key samples (and corresponding bare supports) are reported in Table S5, with a minor loss in surface area found to result from metal deposition and thermal treatment of the catalytic samples.

Author Contributions

R.L. and R.J.L. conducted testing experiments and corresponding data analysis. R.L., D.J.M., and E.K. conducted catalyst characterization and corresponding data processing. R.J.L. and G.J.H. contributed to the design of the study and provided technical advice and result interpretation. T.S. provided technical advice. R.L. and R.J.L. wrote the manuscript and Supporting Information, with all authors commenting on and amending both documents. All authors discussed and contributed to the work.

Acknowledgments

The authors wish to thank the Cardiff University electron microscope facility (CCI-EMF), which has been part-funded by the European Regional Development Fund through the Welsh Government and the Wolfson Foundation for the transmission electron microscopy. XPS data collection was performed at the EPSRC National Facility for XPS (“HarwellXPS”), operated by Cardiff University and UCL, under contract No. PR16195. R.L. acknowledges the Chinese Scholarship Council for funding. R.J.L. and G.J.H. are grateful to the Max Planck Centre for Fundamental Heterogeneous Catalysis (FUNCAT) for financial support.

Conflict of Interests

The authors declare no conflict of interest.

Data Availability Statement

The data that support the findings of this study are available in the supplementary material of this article.

Keywords: Gold · Hydrogen peroxide · Iron · Palladium · Phenol oxidation

- [1] A. J. Jamieson, T. Malkocs, S. B. Pierny, T. Fujii, Z. Zhang, *Nat. Ecol. Evol.* **2017**, *1*, 0051.
- [2] E. R. Jones, M. F. P. Bierkens, N. Wanders, E. H. Sutanudjaja, L. P. H. van Beek, M. T. H. van Vliet, *Commun. Earth Environ.* **2022**, *3*, 221.
- [3] T. A. Larsen, S. Hoffmann, C. Lüthi, B. Truffer, M. Maurer, *Science* **2016**, *352*, 928–933.
- [4] D. Negrete-Bolagay, C. Zamora-Ledezma, C. Chuya-Sumba, F. B. De Sousa, D. Whitehead, F. Alexis, V. H. Guerrero, *J. Environ. Manag.* **2021**, *300*, 113737.
- [5] X. Li, X. Shen, W. Jiang, Y. Xi, S. Li, *Ecotoxicol. Environ. Saf.* **2024**, *278*, 116420.
- [6] E. Svensson Grape, A. J. Chacón-García, S. Rojas, Y. Pérez, A. Jaworski, M. Nero, M. Åhlén, E. Martínez-Ahumada, A. E. Galetsa Feindt, M. Pepillo, M. Narongin-Fujikawa, I. A. Ibarra, O. Cheung, C. Baresel, T. Willhammar, P. Horcjada, A. K. Inge, *Nat. Water* **2023**, *1*, 433–442.
- [7] Z. Wu, Z. Xiong, B. Huang, G. Yao, S. Zhan, B. Lai, *Nat. Commun.* **2024**, *15*, 7775.
- [8] X. Chen, W. Fu, Z. Yang, Y. Yang, Y. Li, H. Huang, X. Zhang, B. Pan, *Water Res.* **2023**, *230*, 119562.
- [9] Z. Liang, Q. Yan, H. Ou, D. Li, Y. Zhang, J. Zhang, L. Zeng, M. Xing, *Proc. Natl. Acad. Sci. USA* **2024**, *121*, e2317394121.
- [10] L. Pi, J. Cai, L. Xiong, J. Cui, H. Hua, D. Tang, X. Mao, *Chem. Eng. J.* **2020**, *389*, 123420.
- [11] S. Esplugas, J. Giménez, S. Contreras, E. Pascual, M. Rodríguez, *Water Res.* **2002**, *36*, 1034–1042.
- [12] H. J. H. Fenton, *J. Chem. Soc., Trans.* **1894**, *65*, 899–910.
- [13] Y. Zhu, R. Zhu, Y. Xi, J. Zhu, G. Zhu, H. He, *Appl. Catal., B* **2019**, *255*, 117739.
- [14] D. W. Flaherty, *ACS Catal.* **2018**, *8*, 1520–1527.
- [15] G. Gao, Y. Tian, X. Gong, Z. Pan, K. Yang, B. Zong, *Chin. J. Catal.* **2020**, *41*, 1039–1047.
- [16] Z. Jin, L. Wang, E. Zuidema, K. Mondal, M. Zhang, J. Zhang, C. Wang, X. Meng, H. Yang, C. Mesters, F.-S. Xiao, *Science* **2020**, *367*, 193–197.
- [17] G. Sharp, R. J. Lewis, G. Magri, J. Liu, D. J. Morgan, T. E. Davies, Á. López-Martín, D. M. Murphy, A. Folli, L. Chen, X. Liu, G. J. Hutchings, *Green Chem.* **2025**, *27*, 5567–5580.
- [18] R. J. Lewis, K. Ueura, X. Liu, Y. Fukuta, T. E. Davies, D. J. Morgan, L. Chen, J. Qi, J. Singleton, J. K. Edwards, S. J. Freakley, C. J. Kiely, Y. Yamamoto, G. J. Hutchings, *Science* **2022**, *376*, 615–620.
- [19] T. Richards, J. H. Harthy, R. J. Lewis, A. G. R. Howe, G. M. Suldecki, A. Folli, D. J. Morgan, T. E. Davies, E. J. Loveridge, D. A. Crole, J. K. Edwards, P. Gaskin, C. J. Kiely, Q. He, D. M. Murphy, J.-Y. Maillard, S. J. Freakley, G. J. Hutchings, *Nat. Catal.* **2021**, *4*, 575–585.
- [20] R. Underhill, R. J. Lewis, S. J. Freakley, M. Douthwaite, P. J. Miedziak, O. Akdim, J. K. Edwards, G. J. Hutchings, *Johns. Matthey Technol. Rev.* **2018**, *62*, 417–425.
- [21] A. Santos, R. J. Lewis, D. J. Morgan, T. E. Davies, E. Hampton, P. Gaskin, G. J. Hutchings, *Catal. Sci. Technol.* **2021**, *11*, 7866–7874.
- [22] W. Liu, L. Tian, L. Shi, *J. Phys. Chem. C* **2024**, *128*, 6682–6688.
- [23] J. Li, T. Ishihara, K. Yoshizawa, *J. Phys. Chem. C* **2011**, *115*, 25359–25367.
- [24] J. Wei, S. Wang, J. Wu, D. Cao, D. Cheng, *Ind. Chem. Mater.* **2024**, *2*, 7–29.
- [25] A. Santos, R. J. Lewis, G. Malta, A. G. R. Howe, D. J. Morgan, E. Hampton, P. Gaskin, G. J. Hutchings, *Ind. Eng. Chem. Res.* **2019**, *58*, 12623–12631.
- [26] R. J. Lewis, K. Ueura, Y. Fukuta, S. J. Freakley, L. Kang, R. Wang, Q. He, J. K. Edwards, D. J. Morgan, Y. Yamamoto, G. J. Hutchings, *ChemCatChem* **2019**, *11*, 1673–1680.
- [27] N. M. Wilson, P. Priyadarshini, S. Kunz, D. W. Flaherty, *J. Catal.* **2018**, *357*, 163–175.
- [28] J. K. Edwards, S. J. Freakley, A. F. Carley, C. J. Kiely, G. J. Hutchings, *Acc. Chem. Res.* **2014**, *47*, 845–854.
- [29] N. M. Wilson, D. W. Flaherty, *J. Am. Chem. Soc.* **2016**, *138*, 574–586.
- [30] R. Li, R. J. Lewis, Á. López-Martín, D. J. Morgan, T. E. Davies, D. Kordus, A. I. Dugulan, B. R. Cuenya, G. J. Hutchings, *Green Chem.* **2025**, *27*, 2065–2077.
- [31] A. Barnes, R. J. Lewis, D. J. Morgan, T. E. Davies, G. J. Hutchings, *Catal. Sci. Technol.* **2022**, *12*, 1986–1995.
- [32] X. Gong, R. J. Lewis, S. Zhou, D. J. Morgan, T. E. Davies, X. Liu, C. J. Kiely, B. Zong, G. J. Hutchings, *Catal. Sci. Technol.* **2020**, *10*, 4635–4644.
- [33] A. Santos, R. J. Lewis, D. J. Morgan, T. E. Davies, E. Hampton, P. Gaskin, G. J. Hutchings, *Catal. Sci. Technol.* **2022**, *12*, 2943–2953.
- [34] W. Li, L. Chen, M. Qiu, W. Li, Y. Zhang, Y. Zhu, J. Li, X. Chen, *ACS Catal.* **2023**, *13*, 10487–10499.
- [35] Z. Kozmér, E. Takács, L. Wojnárovits, T. Alapi, K. Hernádi, A. Dombi, *Radiat. Phys. Chem.* **2016**, *124*, 52–57.
- [36] R. Burch, P. R. Ellis, *Appl. Catal., B* **2003**, *42*, 203–211.

Manuscript received: August 14, 2025

Revised manuscript received: September 8, 2025

Accepted manuscript online: September 9, 2025

Version of record online: ■■, ■■